Available online at www.sciencedirect.com
SCIENCE DIRECT®
Journal of Nuclear Materials 335 (2004) 471–486
journal of nuclear materials
www.elsevier.com/locate/jnucmat

Deformation mode maps for tensile deformation of neutron-irradiated structural alloys

K. Farrell, T.S. Byun *, N. Hashimoto

Metals and Ceramics Division, Oak Ridge National Laboratory, P.O. Box 2008, MS-6151, Oak Ridge, TN 37831, USA

Received 7 June 2004; accepted 17 August 2004

Abstract

The deformation microstructures of neutron-irradiated nuclear structural alloys, A533B steel, 316 stainless steel, and Zircaloy-4, have been investigated by tensile testing and transmission electron microscopy to map the extent of strain localization processes in plastic deformation. Miniature specimens with a thickness of 0.25 mm were irradiated to five levels of neutron dose in the range 0.0001–0.9 displacements per atom (dpa) at 65–100 °C and deformed at room temperature at a nominal strain rate of $10^{-3}\,s^{-1}$. Four modes of deformation were identified, namely three-dimensional dislocation cell formation, planar dislocation activity, fine scale twinning, and dislocation channel deformation (DCD) in which the radiation damage structure has been swept away. The modes varied with material, dose, and strain level. These observations are used to construct the first strain-neutron fluence-deformation mode maps for the test materials. Overall, irradiation encourages planar deformation which is seen as a precursor to DCD and which contributes to changes in the tensile curve, particularly reduced work hardening and diminished uniform ductility. The fluence dependence of the increase in yield stress, $\Delta YS = \alpha(\varphi t)^n$ had an exponent of 0.4–0.5 for fluences up to about $3 \times 10^{22}\,n\,m^{-2}$ (~0.05 dpa) and 0.08–0.15 for higher fluences, consistent with estimated saturation in radiation damage microstructure but also concurrent with the acceleration of gross strain localization associated with DCD.

1. Introduction

During plastic deformation of crystalline metals, the interaction and tangling of dislocations on intersecting slip planes causes resistance to further dislocation movement and requires a higher stress to continue the deformation. Such strain hardening is necessary to continue and extend the deformation in a uniform manner throughout the bulk. Metals that deform in this manner tend to be tough and malleable. On the other hand, if the metal does not deform homogeneously but instead the strain is restricted to a localized region, its mechanical properties are impaired and it may neck or crack prematurely. These grossly contrasting features of uniform and non-uniform plastic deformation can easily be seen in the graphical records of tension tests. Less obvious is an insidious type of strain localization that occurs in pre-hardened metals on a microscopic scale, known as dislocation channel deformation [1–3], and hereinafter

* Corresponding author. Tel.: +1 865 576 7738; fax: +1 865 574 0641.
E-mail address: byunts@ornl.gov (T.S. Byun).

0022-3115/$ - see front matter © 2004 Elsevier B.V. All rights reserved.
doi:10.1016/j.jnucmat.2004.08.006

referred to as DCD. DCD is a process of heterogeneous plastic deformation that entails only a few dislocation sources operating on widely separated slip planes. Dislocations released from the sources glide along the slip planes, cutting through and destroying or assimilating any barriers in their paths. This clearing action creates an easy passageway, or narrow channel a fraction of a micron wide, in which subsequent dislocations from the source can travel easily, and therefore the strain remains confined to the channels. The levels of strain in the channels can be very high, several hundred percent, whereas the bulk strain may be only a few percent [4,5]. Consequently, the strains and stresses at the head of a channel can greatly exceed the applied bulk values and they have the potential for creating new channels or perhaps cracks.

Irradiation with neutrons hardens a metal and makes it more prone to DCD [1,2]. Although this has been known since the earliest days of radiation damage studies [6], a full measure of the connection between neutron irradiation hardening, changes in mechanical properties, and strain localization is wanting, particularly in commercial alloys used in the construction of nuclear reactors. One way to establish such correlation is with deformation mode maps. Deformation mode maps originate from the work of Frost and Ashby [7]. In the Ashby maps the deformation behavior of a metal is condensed into a single diagram depicting regions of specific deformation modes in terms of stress-temperature coordinates. Ashby maps have now been extended to other parameters and other fields [8] and have become a valuable tool for matching materials and properties to applications. Recently, Ashby-type maps considering the effects of irradiation have been constructed for fcc and bcc metals [9]. A deformation mode map constructed in terms of strain-dose coordinates focuses more on the radiation effects. So far, such deformation mode-dose maps have been constructed only for two pure, face-centered cubic (fcc) metals, nickel and gold [10]. These mode maps are reproduced in Fig. 1. They outline the boundaries between regimes of uniform deformation occurring by cell formation and regions where deformation occurs locally by DCD. At low fluences, cell formation is dominant at all strains, and in nickel the size of the dislocation cells decreases from 2 to 0.5 μm with increasing strain and increasing fluence. DCD is observed at a fluence of 2×10^{21} n m^{-2}, but only at low strains; at higher strains it switches to cell formation. At the higher fluences, DCD is more persistent and is the dominant mode at all strains at fluences above about 1×10^{22} n m^{-2}.

The goals of the present work are to systematically map the extent of involvement of strain localization processes in plastic deformation of three commercial alloys used for construction of nuclear reactors. The deformation processes are identified by transmission

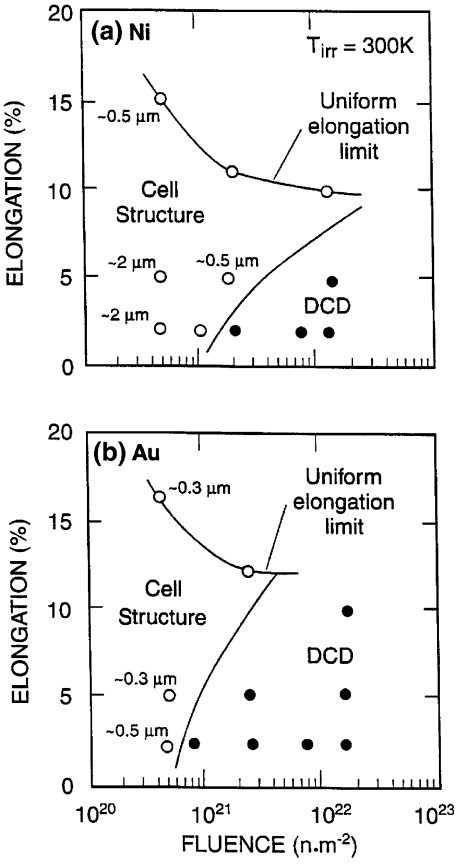

Fig. 1. Deformation mode-fluence maps for nickel and gold irradiated and tensile strained at 300 K [10].

electron microscopy (TEM) examination and related to changes in the tensile properties of the alloys as functions of neutron dose (dpa) and degree of plastic strain.

2. Experiment conditions

The three test materials are a tempered bainitic A533B steel with a matrix of bcc ferrite, typical reactor pressure vessel steel, an annealed 316 stainless steel (fcc) and an annealed Zircaloy-4 (hcp). The last two materials are used for reactor internal components. Chemical compositions of the three alloys, and the heat treatments given to the tensile specimens, are described in Table 1. The miniature sheet tensile specimens had gage section dimensions of 0.25 mm thick, 1.5 mm wide, and 8 mm long [11,12].

Irradiations were conducted in the Hydraulic Tube facility of the High Flux Isotope Reactor. This facility permits small aluminum capsules to be shuttled in and

Table 1
Chemical compositions and heat treatments for test materials

Materials	Chemical composition (wt%)	Heat treatment (in vacuum unless specified)
A533B	Fe–0.22C–0.25Si–1.48Mn–0.52Mo–0.68Ni–0.018S–0.012P	Annealed at 880 °C for 4 h and air cooled, tempered at 660 °C for 4 h, reheat at 610 °C for 20 h
Zr-4	Zr–1.4Sn–0.015C–0.1Fe–0.001S–0.06O–<0.1Ni–<0.001N	Annealed at 670 °C for 30 min
316	Fe–0.059C–1.86Mn–0.57Si–0.018S–0.024P–17.15Cr–13.45Ni–2.34Mo–0.1Cu–0.02Co–0.031N	Annealed at 1050 °C for 30 min

out of the reactor core on demand in a stream of coolant water while the reactor is at power. Gamma heat generated in the capsule is carried away by the hydraulic flow: The irradiation temperature for the specimens (<100 °C) was obtained by irradiating the specimens in direct contact with the flowing coolant water using capsules with many perforations through their walls. The temperature of the specimens was estimated to be in the range 65–100 °C. The irradiation exposures ranged from 5.9×10^{20} n m^{-2} to 5.5×10^{24} n m^{-2} ($E > 1$ MeV) encompassing five discrete levels. Corresponding nominal atomic displacement levels ranged from 0.0001 dpa to 0.89 dpa for the A533B steel and from 0.00009 to 0.8 dpa for the 316 stainless steel and Zircaloy-4 [11].

All tensile tests were performed at room temperature in a screw-driven Instron machine at a crosshead speed of 0.008 mm s^{-1}, corresponding to a specimen strain rate of 10^{-3} s^{-1}. Engineering strain was calculated from the recorded crosshead separation using a nominal gauge length of 8 mm. To exclude the effect from the load train compliance in the stress–strain curves, only the plastic component of strain (elongation) was extracted, and the total strain was obtained by adding the plastic strain to the theoretical elastic strain. Engineering stress was calculated as the load divided by the initial cross sectional area before irradiation.

For each alloy, at least two specimens were tested to failure at each dose level to obtain a full tensile curve and complete tensile properties. Tests on other specimens at the same dose were curtailed at prescribed strains and the gauge sections of the specimens were sectioned for TEM study. The TEM pieces cut from the gauge sections of the tensile specimens were rectangular with dimensions of only $1.5 \times 1.5 \times 0.25$ mm, which is much smaller than a standard 3 mm diameter TEM disk. Preparation of electropolished TEM foils from these small pieces in a Tenupol electropolishing apparatus required substantial development work and modification of Tenupol specimen holders. Note that TEM micrograph was not produced at some strains and doses because there were difficulties in the preparation of thin foils, or the microstructure was believed to be unchanged from the unirradiated material. Microstructures were observed in a JEM-2000FX transmission electron microscope operating at 200 kV. Experimental details are given elsewhere [11,12].

3. Results

3.1. A533B steel

TEM study of the unirradiated specimens revealed microstructures consisting of packets of lath-like grains divided into equiaxed subgrains about 300–1000 nm size and containing many tangled dislocations [11]. Numerous carbide particles of sizes 50–500 nm were distributed randomly through the matrix. In the as-irradiated specimens, no radiation-induced defect structure (RDS) was discernable for doses of about 0.0001, 0.001, 0.01, and 0.1 dpa [11]. For the 0.89 dpa dose, RDS was clearly visible as distinct black spot defects. Note that in all the materials examined in this work, some of these black spots are small dislocation loops, not all of which are visible in a given beam direction. To observe most of the defect clusters, they were measured in weak-beam dark-field conditions but no attempt was made to determine the invisible fractions.

Measurements of the defects in the A533B steel at 0.89 dpa gave a concentration of 6.5×10^{22} m^{-3} and a mean size of 1.3 nm. (For brevity, the as-irradiated microstructures are not included in this paper, as the same features can be seen in the as-deformed microstructures, which are the main results of the present experiments. More detailed results are presented in Ref. [11].)

The effects of neutron fluence on the tensile properties of the A533B ferritic pressure vessel steel are presented in Fig. 2 and Table 2. Fig. 2 contains typical tensile test curves. The yield point drop and the associated region of elongation at constant stress, the Lüders region, for the unirradiated specimen are characteristic of ferritic steel. The yield strength (YS) and the ultimate tensile strength (UTS) are presented in Table 2, as well as the uniform elongation (UE) and the total elongation (TE).

It can be seen that for the two lowest doses of 0.0001 and 0.001 dpa there are small increases in YS and UTS, and small reductions in elongation. The increases in YS and UTS are about equal, which means that irradiation to these low doses did not alter the work hardening behavior. At the middle dose of 0.01 dpa, the increase in

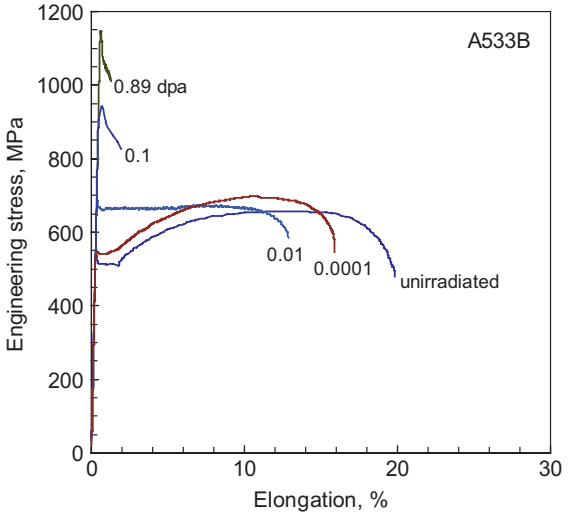

Fig. 2. Representative tensile test curves for A533B steel after different neutron exposures.

YS and decrease in elongation are more pronounced and the work hardening region is eliminated, being replaced by a lengthy Lüders-like region that terminates in necking failure. The YS is increased by about 35% and is almost equal to the UTS, which is about the same value as the UTS values for the lower doses. For the two higher doses of 0.1 and 0.89 dpa, the UTS and YS are indistinguishable but are considerably higher than for the lower doses; there is no engineering work hardening, and prompt terminal plastic instability begins at yield.

With regard to deformation microstructures observed in the deformed specimens, the mode of deformation appeared to be multiple slip and dislocation tangling in the unirradiated A533B specimens and in the two lower dose specimens, Fig. 3(a) and (b). No DCD was discerned. At 0.01 dpa the deformation mode was still predominantly dislocation tangles. At doses of 0.1 and 0.89 dpa, where large increases in yield stresses accompanied by prompt plastic instability failures were found, it was difficult to characterize the deformation mode because the strain was so strongly localized in a single neck that most of the TEM sections cut from the gauge length were barely strained whilst those TEM pieces taken from the highly necked fracture region were of unsuitable shape for electrothinning. Hence, although a few dislocation channels were observed, they were insufficient for statistical analysis. Several channels are shown in Fig. 4(a) and (b). They are about 30 nm wide. The channels pass undeflected through the laths but change direction at the former bainite packet boundaries. The deformation mode map derived for A533B steel from these observations is shown in Fig. 5.

Table 2
Engineering tensile data at room temperature after irradiation at temperatures in the range 60–100 °C

ID	Materials	dpa	YS (0.2% offset) (MPa)	UTS (MPa)	UE (%)	TE (%)
a77	A533B	0	459	595	12.5	17.8
a78		0	501	640	12.9	19.6
a85		0	512	652	11.5	20.6
a76		0	514	656	13	19.5
a34		0.0001	517	659	12.1	17.5
a35		0.0001	541	698	10.2	15.3
a22		0.001	506	636	12.3	18
a15		0.001	523	666	10.7	16.8
a14		0.001	528	684	10.9	16.4
a32		0.01	661	668	8.4	12.5
a33		0.01	678	692	7.8	13.1
a47		0.1	931	931	0	0.2
a48		0.1	935	935	0	0.3
a49		0.1	942	942	0	1.3
a40		0.89	1003	1003	0	1
a39		0.89	1043	1043	0	1.2
r74	Zr-4	0	378	434	12.3	29
r75		0	388	447	12	33.2
r83		0	415	471	12.3	28.2
r76		0	404	473	15	36.4
r13		0.00009	396	460	12.7	30.2
r12		0.00009	411	481	14.4	29.8
r14		0.0009	438	477	8.4	26.7
r18		0.0009	438	478	9.8	24.3
r30		0.009	521	514	3.2	16.3
r24		0.009	520	519	2.7	17
r50		0.09	560	584	0	17
r35		0.8	594	594	0	8.8
r34		0.8	601	601	0	9.8
t91	316SS	0	217	562	55.2	62.8
t80		0	237	572	54.2	56.3
t78		0	240	588	54.3	58.3
t76		0	243	593	58.7	61.6
t05		0.0001	256	609	57	59.6
t06		0.0001	288	695	63.1	67
t15		0.001	316	631	51.8	55
t17		0.001	354	677	52.7	59
t55		0.01	448	667	37.3	39.5
t21		0.01	449	682	38.1	40
t56		0.01	501	706	44.3	47.6
t22		0.01	470	714	38	42.8
t75		0.1	567	735	37	41.3
t81		0.1	574	740	35.1	39.1
t37		0.78	676	779	28.8	30
t32		0.78	672	788	32.6	36.1

3.2. Zircaloy-4

The microstructure of unirradiated Zircaloy-4, hereafter abbreviated to Zr-4, consisted of equiaxed grains containing a few grown-in dislocations. In the as-irradi-

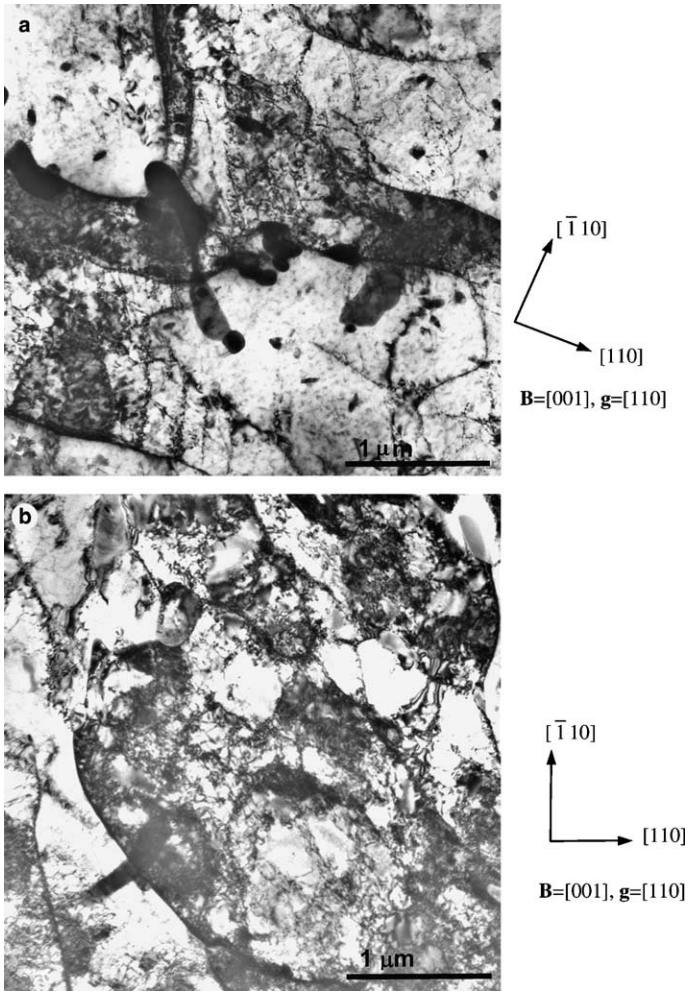

Fig. 3. Deformation microstructure in unirradiated and low dose A533B steel specimens: (a) at 0 dpa after 6% strain, and (b) at 0.01 dpa after 10% strain.

ated specimens no RDS was found at a nominal dose of 0.0001 dpa. At 0.001 dpa, fine black spots were just discernable at a concentration of about $1.1 \times 10^{22}\,m^{-3}$ and mean size of 1.2 nm. At the highest dose, 0.8 dpa, black spot damage was quite evident at a concentration of $6.1 \times 10^{22}\,m^{-3}$ and mean size 1.4 nm [11].

The changes in tensile properties of Zr-4 with dose are listed in Table 2. Fig. 6 displays typical tensile test curves for Zr-4. Characteristically, annealed unirradiated Zr-4 does not display a yield point drop, and none are found in the unirradiated specimens and in those irradiated to low doses of 0.0001 and 0.001 dpa. These low doses raise the YS and UTS, but do not significantly alter the work hardening rate. At a nominal dose of 0.01 dpa, the increase in YS is much larger than at the lower doses and a weak yield point drop is seen. The engineering work hardening rate is negative but failure is not immediate; it is extended over a necking elongation of almost 20%. The curve for the nominal 0.1 dpa dose is very similar to that for 0.01 dpa except for a higher YS and a much stronger yield point drop. Again, necking is drawn out over about 18% elongation. For 0.1 dpa, and for the highest dose of 0.8 dpa, a yield point drop is prominent and there is no uniform strain region; necking is diffuse but is without bumps. The necking strain for the 0.8 dpa specimen is reduced but is nevertheless a substantial 10%.

After plastic deformation, the unirradiated specimens and the two lower dose specimens of Zr-4 contain widely-spaced bands of elongated dislocations lying mainly in the prismatic $\{1\,0\,\bar{1}\,0\}\langle 1\,1\,\bar{2}\,0\rangle$ slip system, with a small amount in the pyramidal $\{1\,0\,\bar{1}\,1\}\langle 1\,1\,\bar{2}\,0\rangle$ system, Figs. 7 and 8. No DCD is found at low doses. In the 0.01 dpa specimens, the strain dislocations are still in widely separated bands but now the secondary, $\{1\,0\,\bar{1}\,1\}\langle 1\,1\,\bar{2}\,0\rangle$ system, is more strongly involved [11].

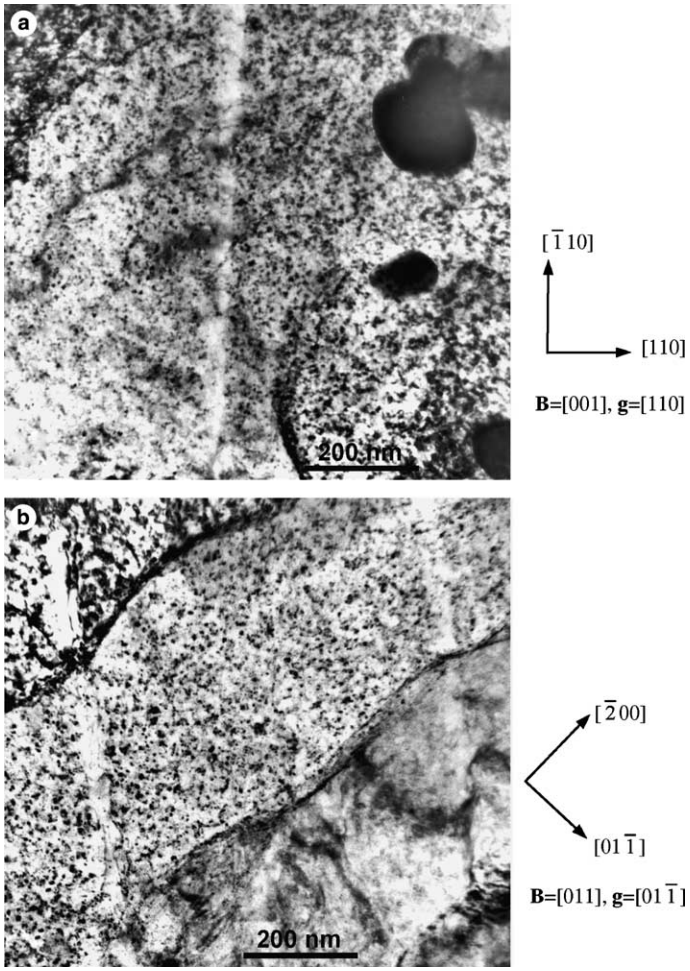

Fig. 4. Dislocation channels in A533B steel: (a) and (b) from different places, at 0.89 dpa after 0.2% strain. Defect clusters (black dots) are evident at this dose.

The dislocations in the major slip bands are lying in channels, Fig. 8(a), seen as white bands after slightly tilting the specimen to put the contained dislocations out of contrast. The channel edges are not sharp, and the channel contrast is not strong, suggesting that there are remnants of RDS in them. Channel widths varied from barely perceptible lines to about 100 nm. The spacing between the wider channels was roughly 500 nm, and the narrower channels were contained between them. Assuming the larger channels to be created first, their presence obviously did not inhibit the formation of new channels.

At 0.1 dpa and 0.8 dpa, the dislocation channels were much more obvious, as seen in Fig. 8(b). Within individual grains there tended to be only one slip system, $\{1\,0\,\bar{1}\,0\}\langle 1\,1\,\bar{2}\,0\rangle$, and cross channels were rare. The major channels were uniformly 40–75 nm wide and were spaced at 400–1100 nm. Between the major channels were relatively few narrow ones, <30 nm wide. The deformation mode map derived for annealed Zr-4 from these observations is shown in Fig. 9.

3.3. 316 Stainless steel

The microstructure of as-annealed 316 steel consisted of equiaxed grains containing some large annealing twins [11]. After irradiation black spot RDS was clearly evident. A relatively low defect cluster density, $\sim 1\times10^{22}\,m^{-3}$, was measured at the lowest dose of 0.0001 dpa. For higher doses, cluster densities were on the order of $1\times10^{23}\,m^{-3}$, and they increased by a factor of about 5 over the dose range 0.001 to 0.8 dpa. The mean size of the clusters varied little with dose and was about 1.6 nm.

The dose dependence of the tensile properties is summarized in Table 2, and representative tensile test curves

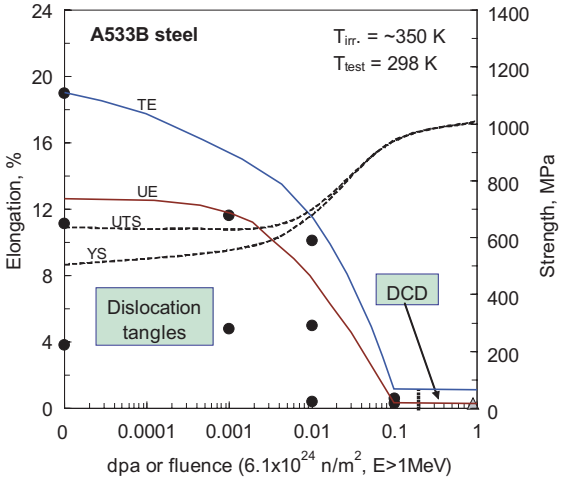

Fig. 5. Deformation mode map for A533B steel neutron-irradiated at 65–100 °C and tested at room temperature.

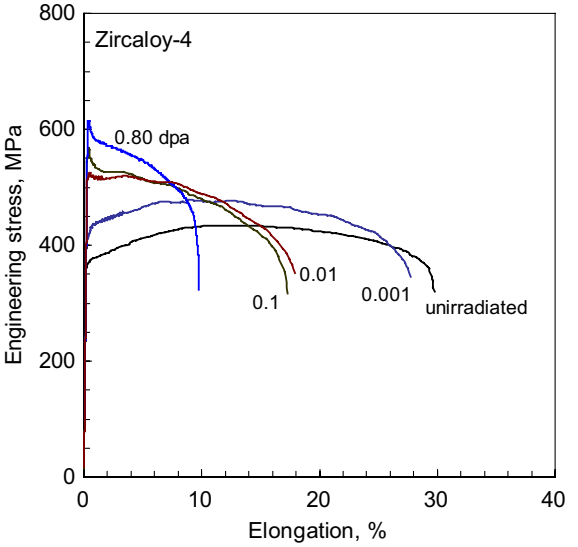

Fig. 6. Representative tensile test curves for Zircaloy-4 after different neutron exposures.

for the annealed 316 stainless steel specimens are displayed in Fig. 10. The curves are very similar to those reported for 304, 316, and 347 stainless steel irradiated elsewhere at ~50 °C to similar doses with larger specimens [13]. In that study there was no yield point drop in the unirradiated materials and in those irradiated to the lower fluences. A yield point drop appeared at a fluence of about 6×10^{22} n m^{-2} (~0.01 dpa) and increased in size with increasing dose. In the present study the 316 steel behaves in the same way. There is a small yield inflection but no yield point drop in the unirradiated material and at the two lower fluences. The yield stress is raised slightly by the irradiation and the elongation is decreased by a small amount, but there is not much effect on the work hardening rate. At the higher doses, there is substantial increase in YS. However, the elongation suffers only relatively mild loss, in sharp contrast to the large ductility losses seen in the A533B steel and to a less degree in the Zr-4. There is no strain softening (apparent negative work hardening) and no prompt plastic instability failure in the stainless steel, even at the highest dose.

With regard to deformation mode, the unirradiated 316 steel deforms by slip on $\{1\,1\,1\}\langle 1\,1\,0\rangle$ systems. At low strains of 1% or so, the dislocations

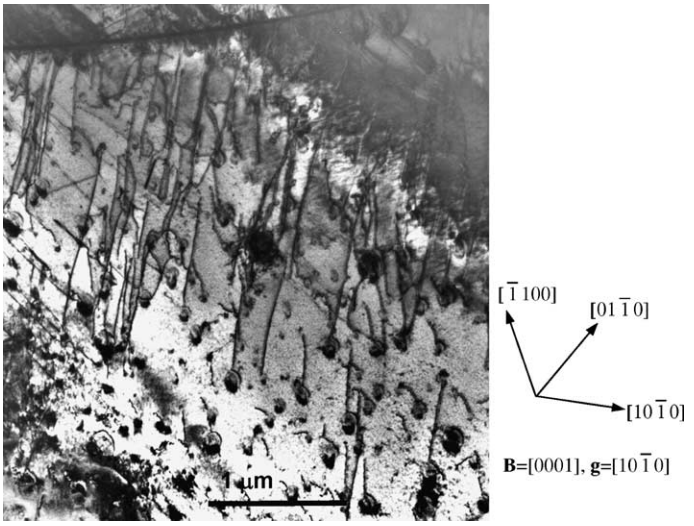

Fig. 7. Typical dislocation structure in unirradiated, deformed Zircaloy-4 after 3% strain.

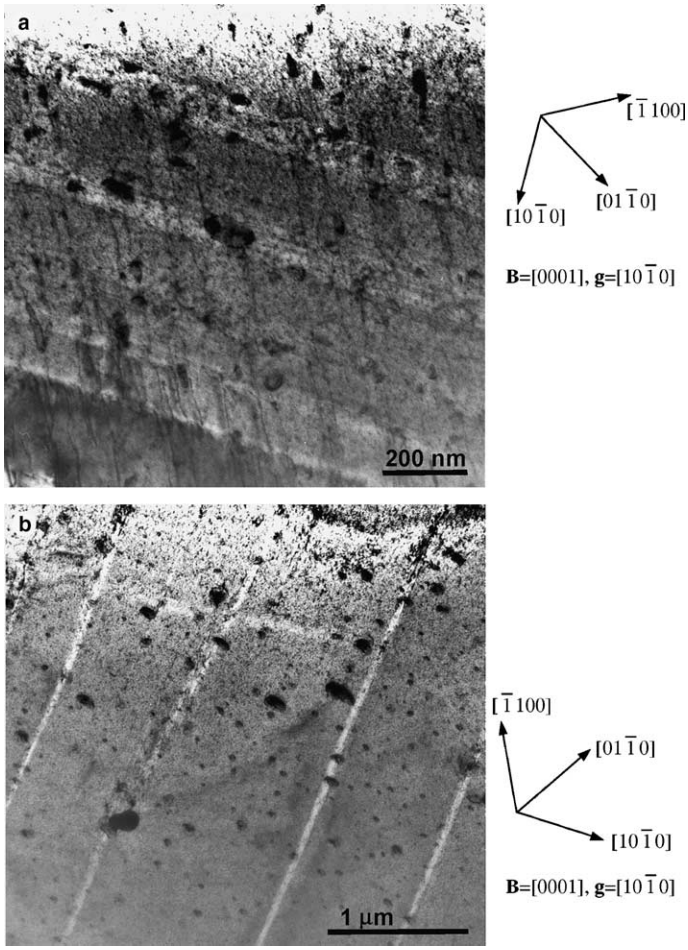

Fig. 8. Deformation microstructures in irradiated Zircaloy-4: (a) dislocation arrays with early channels at 0.009 dpa after 4.8% strain, and (b) fully-developed channels at 0.8 dpa after 6.3% strain.

are primarily in planar arrays, Fig. 11(a). Short lengths of stacking fault fringes are frequently visible in the dislocations. As the strain level increases the arrays thicken into bands on $\{1\,1\,1\}\langle 1\,1\,0\rangle$, and random, tangled dislocations appear in the matrix between the bands [14–17]. With increasing strain, the slip bands became more pronounced and at about 5% elongation, the appearance of streaks in electron diffraction patterns indicated the occurrence of fine twins. Dark field illumination using the twin streaks placed the fine twins in the slip bands. Such fine deformation twins are created by overlapping of the stacking faults of extended dislocations on consecutive slip planes in the slip bands, as described in references [14–17]. This twinning is not an instantaneous blocky shear process, and no twinning discontinuities are seen in the stress–strain curves. At high strains of 50% or so, the twins are very evident in the microstructure, Fig. 11(b).

After irradiation to the two lower doses, no change in deformation mode was observed. At doses up to 0.01 dpa, there was still no appreciable distinction between the deformation modes for unirradiated and irradiated specimens. Even at the higher doses there is no radical change in deformation mode; rather, the nature of the deformation remains the same but the degree of damage is altered subtly. Twins show up in the dislocation bands at lower strains than in the unirradiated specimens. At a dose of about 0.1 dpa, the dislocation bands are replaced by narrow channels in which the RDS has been largely erased, Fig. 12(a). Most of the channels contain deformation twins and some glide dislocations, but a small portion of the channels seem to be clear of all structure no matter how much the TEM specimen is tilted in attempts to reveal features in the channels. This coexistence of twins and channels has been explained by a stress-based deformation twinning theory [17]. Offsets are seen at channel intersections, and there

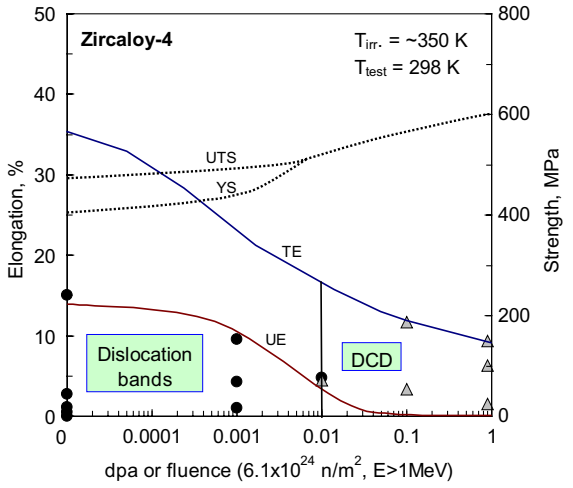

Fig. 9. Deformation mode map for Zircaloy-4 neutron-irradiated at 65–100 °C and tested at room temperature.

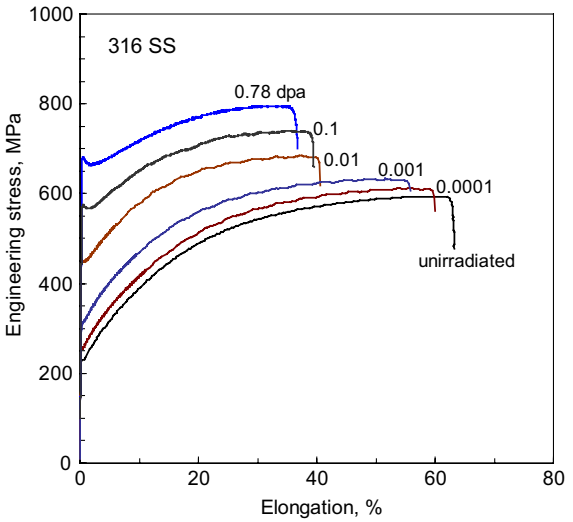

Fig. 10. Representative tensile test curves for 316 stainless steel after different neutron exposures.

is substantial dislocation activity at the junctions. Furthermore, some of the clear channels are curved, departing at an angle of about 7.5° from the major channels. Numerous short cross channels, like ladder rungs, connect the major channels, Fig. 12. There are tangled dislocations in the spaces between the channels, and their presence does not seem to have affected the black spot RDS there. Many of the channels are present in the earliest stages of straining, and they proliferate with strain. Large stacking faults and twins are present in the channels even at low strain levels. At the highest dose of 0.79 dpa, the channels carve the deformation microstructure into subdivided rhombohedral blocks, Fig. 12(b). Considerable grain-to-grain variation was found in the channel widths and spacings. Even within a single grain there was high variability. Despite these variations it was observed that both the channel width and the spacing increase with dose, indicating fewer but wider channels at the higher doses [11]. The deformation mode map derived for annealed 316 austenitic stainless from these observations is shown in Fig. 13.

4. Discussion

4.1. Deformation mode maps for different alloys

This work has produced the first ever deformation mode maps for reactor structural alloys neutron irradiated at about 100 °C and tensile tested at room temperature, shown in Figs. 5, 9, and 14 for A533B steel, Zr-4, and 316 stainless steel, respectively. These maps identify the major modes of plastic deformation operating during tensile tests of irradiated materials at room temperature. The boundaries of the deformation regimes are outlined in terms of neutron fluence and plastic elongation. The data are sparse but they provide the framework for subsequent refinement as more data become available.

In the maps, four deformation modes are recognized; namely, dislocation tangling and cell formation; banding or planar deformation; dislocation channel deformation (DCD); and deformation microtwinning. Deformation by dislocation tangling and cell formation is the normal mode in most unirradiated metals. It develops from a three-dimensional interaction of dislocations resulting from cross slip and impingement of dislocations on intersecting slip planes. It occurs to some extent in all three materials herein, whether irradiated or not. It is the dominant mode in the A533B steel for doses below 0.1 dpa. It competes with DCD and is suppressed when DCD is strong. Dislocation banding, or planar deformation, represents confinement of dislocation activity to a limited number of slip planes. It is a normal mode of deformation where a single slip system is dominant, as in Zr-4, or where dislocation cross slip is diminished, as in the 316 steel. Diminished cross slip is a consequence of the low stacking fault energy of austenitic steel, as discussed later. Planar dislocation deformation is encouraged by irradiation, and when developed after irradiation such planar deformation is considered to be a precursor of DCD. However, a prior propensity for planar deformation in the unirradiated condition is not a prerequisite for DCD, as evidenced by reports of DCD in copper [14,18], nickel [10,19], and niobium [5] which are not normally prone to planar deformation. DCD is not found in any of the three alloys before irradiation. It is seen in all three alloys after irradiation, but

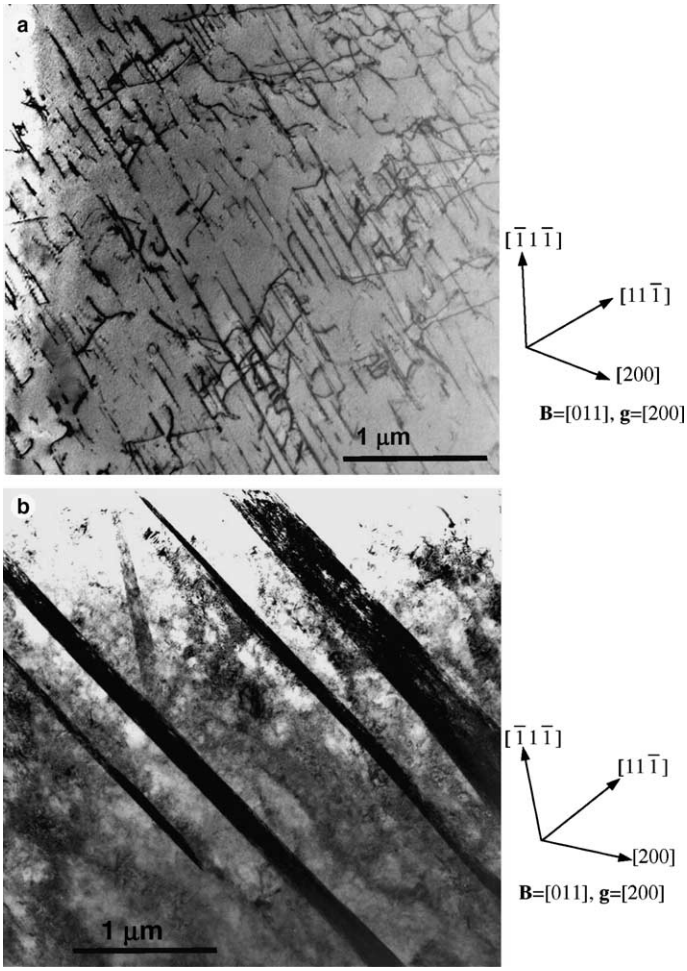

Fig. 11. Planar deformation in unirradiated 316 stainless steel strained 1.5% at room temperature in (a); and deformation twins in the same steel strained 54% at room temperature in (b).

not at the lower neutron fluences. Deformation microtwinning is seen only in the austenitic steel. It occurs before and after irradiation and is a result of low stacking fault energy, and is encouraged by irradiation [14–17]. It is also known that the deformation mechanism changes from twinning dominant to channeling dominant process with increasing test and irradiation temperatures [20,21].

Finding a dose threshold for DCD for each material should be a key objective in mapping deformation modes. The minimum dose at which DCD begins in the three materials for irradiation at 65–100 °C is about 0.01 dpa for Zr-4 and A533B steel, and between 0.01 and 0.1 dpa for the stainless steel. The occurrence of DCD in pure nickel and gold [10] under 14 MeV neutron irradiation begins at a fluence of about 1×10^{21} n m^{-2}. A D–T neutron fluence of 1×10^{21} n m^{-2} corresponds to about 0.004 dpa for medium atomic mass number metals like nickel [19]. For such high-energy neutrons, the atomic displacement cross sections are about ten times larger than for fission neutrons with energies >1 MeV. Hence, the threshold displacement doses for DCD in the present alloys are 2.5–25 times higher than the thresholds for pure nickel and gold. Some of this difference may be due to differences in irradiation parameters such as neutron spectrum and damage rate. But most of the difference is probably attributable to differences in chemical composition. The alloying additions and impurity elements in the alloys may reduce survival of point defects from displacement cascades and may promote greater recombination of freely migrating point defects, thereby reducing the development of RDS. Attainment of a critical yield stress for initiation of DCD would then be delayed to higher doses. Actually, it is not known what triggers DCD, whether it is achievement of a critical stress

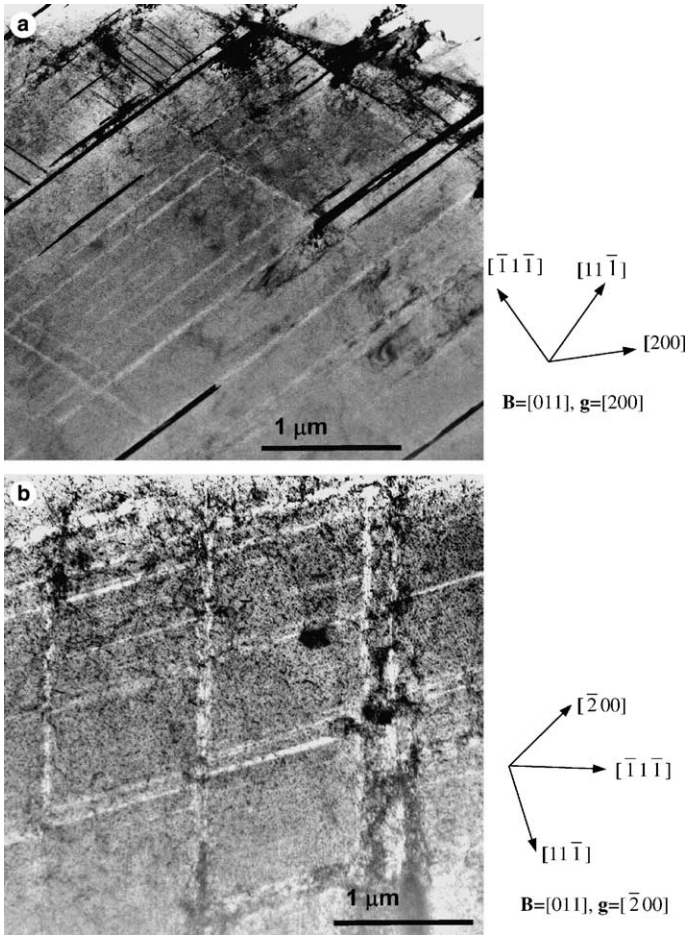

Fig. 12. Mixture of twins and dislocation channels in 316 stainless steel irradiated to 0.15 dpa and strained 6% in (a); and intersecting arrangement of dislocation channels in 316 stainless steel irradiated to 0.78 dpa and strained 32% in (b).

greater than the unirradiated yield strength, or a critical softening stress due to defect clearing.

4.2. Dislocation channeling and tensile curve behavior

Regarding the engineering tensile curves and tensile properties, a pattern is noted in which changes in properties induced by irradiation near room temperature fall into two regimes of fluence dependence. The first regime is at low fluences and is characterized by minor reductions in elongations and by small increases in yield strengths without introduction of yield point drops. In this regime, the deformation modes are the same as those for the unirradiated material; work hardening rates are unchanged, and there are no overt signs of DCD. The second regime is at fluences of 0.01 dpa and higher, and is distinguished by large increases in yield strengths, introduction or enhancement of yield point drops, large decreases in elongations, and significant reductions in macroscopic work hardening rates. In this higher fluence regime, DCD is involved. In the 316 steel, there is increased microtwinning activity in addition to the DCD. For all three alloys the losses in ductility due to irradiation are associated primarily with reductions in uniform elongation. Except for the A533B steel at the two highest doses, the necking strains (i.e. the differences between the total elongation and the uniform elongation) are barely affected by the irradiation. The implication is that the tensile properties are most impacted by the changes in the work hardening regions prior to reaching the UTS.

It is seen that DCD is the only deformation mode induced by irradiation in three materials. Furthermore, the incidence of DCD coincides most closely with the larger irradiation-induced changes in the tensile curves. That coincidence is not accidental. It represents an intimate connection between channeling and the alteration of tensile properties, in conformation with similar

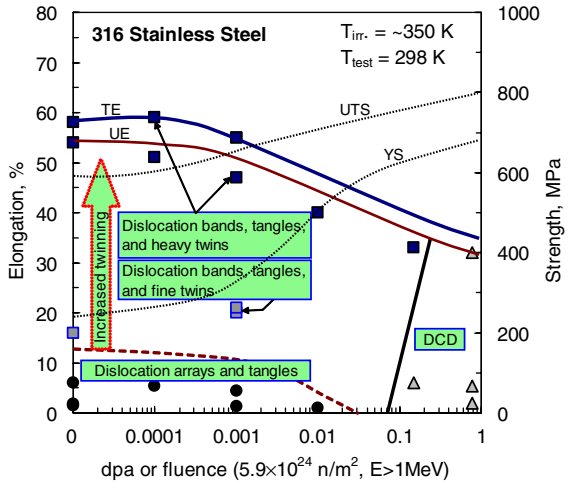

Fig. 13. Deformation mode map for 316 austenitic stainless steel neutron-irradiated at 65–100 °C and tested at room temperature.

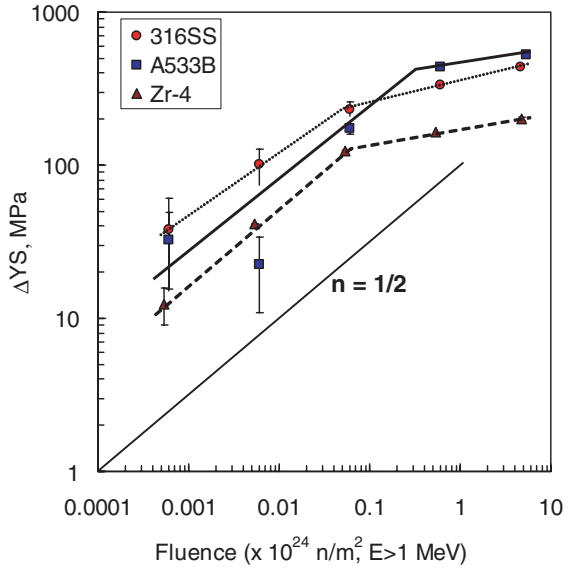

Fig. 14. Determination of radiation hardening exponents for the three alloys.

relationships established elsewhere in both irradiated and unirradiated materials. Strain localization is not peculiar to irradiated materials. It is quite common in unirradiated materials, where it is referred to as work softening. It is usually preceded by a yield point drop, after which deformation initially proceeds locally at low work hardening rate. Work softening involving swept-out dislocation channels is encountered in materials that have been prehardened by cold straining [3,22,23], by quenching [23,24], or by some precipitates [25,26]. Perhaps the best-known example is the strong yield point and related Lüders bands seen in mild steels. The features of non-uniform deformation found in the first tensile tests conducted on a neutron irradiated metal, single crystal copper, reported in detail in 1960 [6], were likened at that time to Lüders bands. The deformation bands in irradiated copper were subsequently shown to be DCD [4,27,28]. Similar findings were subsequently made for irradiated molybdenum [29]. In short, DCD seen in irradiated metals is a facet of the broader phenomenon of work softening.

Explanations of the yield point drop and associated strain localization in work softening are plentiful. They include sudden release of dislocations from locked sources [30], rapid multiplication and movement of dislocations [31], cascade-induced source hardening model [32], geometrical softening [33], and adiabatic heating [5]. The underlying premises are that the prehardening treatments have locked the dislocation sources, which then require higher stresses to activate them. When the first sources are activated they send avalanches of dislocations sweeping through the barriers ahead of them, clearing softened pathways. A general observation is that the higher the yield stress at which plastic strain begins, the greater is the propensity for channeling. It has been proposed [34] that the character of slip correlates more systematically with stress than with any other parameter, and that focused or localized slip is favored by higher stresses. It is also well known that the velocity of glide dislocations increases exponentially with stress [31], which invokes high strain rates in channels. Indeed, high speed photography of the surface slip lines resulting from DCD has shown that they develop very rapidly, in less than a millisecond [18,35]. Details of the barrier clearing process(es) are specific to particular types of barriers and are still very much debatable. It is generally agreed that once the initial channels are formed, less force is required to maintain the imposed strain rate, hence the load, and stress, drops. Under the reduced stress, activation of additional sources is denied and dislocation activity in the surrounding stronger matrix is suppressed; therefore, deformation is restricted to the cleared channel regions until work hardening at channel/channel and channel/grain boundary intersections raises the stress.

It might follow that the occurrence of a yield point drop coupled with reduced work hardening can be a sign of strain localization. However, the opposite is not always true. In irradiated pure nickel [10], for example, none of the specimens that exhibited DCD in TEM displayed a yield point drop or significant reduction in work hardening rate. In pure gold, all the irradiated specimens showed large reductions in work hardening whether they deformed by channeling or not, and only the highest fluence specimen (1.7×10^{22} n m^{-2}, about 0.07 dpa) had a yield point drop [10]. The deformation

mode in the nickel is notable in that it underwent a transition from dislocation cell type to a lamellar or planar band structure before cleared channels emerged. Such banding is, of course, a form of strain localization and can thus be expected to contribute to changes in the tensile curve in a similar manner to channels. It is believed that such a high work hardening rate with microscopically-localized deformation is associated with a rapid buildup of back stress; with which the work softening can be only a local or short-lived phenomenon in the early process of strain localization. This explanation is being studied with detailed modeling.

4.3. Characteristics of deformation mechanisms for different alloys

In the present work, the stainless steel displays some of the dislocation banding, or incipient channeling behavior seen in the microstructural development of the channels in nickel. After a dose of 0.01 dpa a yield point drop is produced in the stainless steel but there is no associated decrease in work hardening rate. No channels are discerned but dislocation banding is more pronounced. At higher doses, dislocation channels are observed and they are narrower than those in the other two alloys at a given dose. Moreover, of the three alloys investigated here, the stainless steel is the only alloy that retains much of the channeling dislocations within the channels. The channels in stainless steel also contain fine microtwins, not seen in the other two alloys.

Because of the low stacking fault energy of austenitic stainless steel, the partial dislocations that constitute a glide dislocation are more widely separated, or extended [14–17,36,37], than in higher stacking fault materials such as the A533B steel and Zr-4. Before a dislocation can move off its primary slip plane onto a cross slip plane the stacking fault between the partials must first be compressed, which requires a higher stress to overcome the repulsive forces between the partial dislocations. Therefore, cross slip is suppressed and the deformation tends to be much more planar in stainless steel than in higher stacking fault materials.

The twins in the strained stainless steel are not the sudden massive shear, blocky type, accompanied by sharp drops in stress that are common in some metals during straining at low temperature. The twins in stainless steel occur gradually by partial dislocation slip and, as shown elsewhere [14–17,19,36,37], they are formed by successive glides on adjacent slip planes. This twinning mechanism results from low stacking fault energy and is probably the main reason why the stainless steel has much more resistance to radiation-induced ductility loss than the other two alloys [17]. The total elongation of the unirradiated stainless steel (63%) is much larger than those of the other two alloys, 20% for A533B and 33% for Zr-4. This superior elongation in the stainless steel stems largely from protracted uniform elongation, which comprises almost all of its total elongation, whereas in the other alloys the uniform elongations represent less than half of their total elongations. The feature that prolongs the uniform elongation of the stainless steel might be the microtwins, which develop within the deformation bands. Both the stainless steel and the Zr-4 deform by dislocation banding, which being a strain localization process should limit their elongation. But only the stainless steel develops microtwins in the bands. And the stainless steel is much more ductile than the Zircaloy. In such narrow bands dislocation pileups occur more readily, which generates more back stress hardening and encourages activation of new slip sources. Additionally, the higher stresses induced by irradiation or deformation cause greater separation of the partials, producing wider stacking faults [17]. These faults are precursors of the deformation twins found in the bands. Since the faults and twins are formed progressively with strain, they can continue to prolong work hardening. On these grounds it is proposed here that the stacking faults and twins are responsible for the superior elongation of the stainless steel in both its irradiated and unirradiated conditions.

Zirconium alloys undergo slip primarily on $\{0\,0\,0\,1\}$ basal, $\{1\,0\,\bar{1}\,0\}$ prism, and $\{1\,0\,\bar{1}\,1\}$ pyramidal planes, in a common $\langle 1\,1\,\bar{2}\,0\rangle$ direction. Mechanical twinning can occur together with slip. No twins were seen in the Zircaloy-4 in the present work, presumably because of a lack of suitable texture. Zirconium alloys develop strong textures during forming operations. In tension tests the dominant deformation mode is dependent on the processing texture. In rolled sheet, the basal planes become aligned in the plane of the sheet and are tilted slightly in the rolling direction. If the tensile specimen is machined in the thickness direction (T type), such that its basal planes lie nearly perpendicular to the tensile axis, it will deform by a mixture of non-basal slip and gross mechanical twinning. Some of the twins will be suitably reoriented for slip to occur in them [38]. If the tensile specimen is taken in the longitudinal forming direction (L type), it will deform primarily by slip. In the present work, the tensile specimens were machined in the rolling direction, L type, and no twins were seen in the tensile tests. In literature reports of DCD in zirconium alloys, some specimens were of T type and they displayed mechanical twinning during tensile testing [38]. The twins were of the massive, lenticular type. Formation of these broad deformation twins did not remove RDS and cause DCD, but slip bands occurring within the twins did. Interestingly, during those tests, which were made after a fluence of $4\times10^{23}\,\mathrm{n\,m^{-2}}$, $E>1\,\mathrm{MeV}$, (about 0.07 dpa) the occurrence of DCD did not seem to be sensitive to material composition; it was found in zirconium iodide, Zircaloy-2, and Zr–2.3Nb.

4.4. Irradiation hardening behavior

A final point of discussion is the increases in yield strength caused by irradiation. Historically, the earliest radiation strengthening data were obtained on copper [6] and were found empirically to fit an equation of the form $\Delta YS = \alpha(\varphi t)^{1/3}$ over a wide range of doses, where ΔYS is the increase in critical shear stress or macro yield strength, and φt is the neutron fluence. It was quickly pointed out [39] that the data could equally well fit the equation with an exponent of 1/2, which was the expectation for a hardening model involving hindrance of glide dislocations on slip planes by a random distribution of point defect clusters. This model assumes that the volume fraction of clusters varies linearly with fluence and that the defect size is constant. This assumption was later challenged when analysis of cluster densities in pure copper [40] indicated they were linear with fluence only at very low fluences below about 5×10^{20} n m^{-2}, corresponding to about 0.0001 dpa, above which they varied with $(\varphi t)^{1/2}$. Subsequent analysis [41] of a broader range of copper data from many sources showed that for doses above about 0.0001 dpa the cluster density exponent might be 1 or 1/2, depending on interstitial impurity content. A cluster exponent of 1/2 would make $\Delta YS = \alpha(\varphi t)^{1/4}$. It is recognized that all of these relationships will fail at higher doses due to saturation in formation of clusters caused by overlapping of displacement cascades and by absorption of freely migrating point defects at existing clusters. For copper, such saturation is estimated to occur at a dose of about 0.1 dpa [40] and has been seen at about that dose [41,42]. For iron, cluster saturation is believed to occur at 0.01–0.04 dpa according to irradiation hardening behavior [43,44] but is not seen until at least 0.5 dpa [42].

The tensile data obtained in the present work afforded an opportunity to test these predictions. In Fig. 14 the increases in yield strengths are plotted against fast neutron fluence in a log–log plot. There are obvious signs of saturation of hardening at the highest fluence, so the data were arbitrarily analyzed as low and high dose regimes. The results of a least squares line-fitting analyses are shown in Table 3. To make the values compatible with literature data, the analysis was done with φt in units of n cm^{-2}, $E > 1$ MeV. At the lower doses the slope is essentially 1/2 for all three materials irrespective of their large differences in crystal structure, chemical composition, and microstructure. At fluences above 6×10^{22}–6×10^{23} n cm^{-2}, corresponding to displacement doses of 0.01–0.1 dpa for all three materials, the hardening exponent is reduced to the order of 0.1.

Usually, such a decrease in hardening exponent would be taken as an indication that saturation of point defect clusters was occurring at doses above 0.01–0.1 dpa [45,46]. That simple explanation is now confounded by the observation herein that the dose range 0.01–0.1 dpa also coincides with a profound change in deformation mode to one dominated by prompt plastic instability at yield, initiated by DCD. A similar change in deformation mode at these doses has recently been found in a number of ferritic steels [45,47], including tempered martensite which has a similar microstructure to our tempered A533B steel, and in various pure metals [48]. Thus the reduced exponent of irradiation hardening at higher doses deduced from measurements of changes in tensile yield strength might be due to a change in deformation mode, which might also be associated with the reduction in production rate of RDS.

Table 3
Fitting parameters for radiation hardening equation $\Delta YS = \alpha(\varphi t)^n$

Alloy	Low dose regime		Higher dose regime	
	α_1	n_1	α_2	n_2
A533B	5.45×10^{-8}	0.43	5.53	0.08
Zr-4	1.26×10^{-9}	0.5	0.54	0.11
316ss	2.43×10^{-7}	0.4	0.11	0.15

5. Summary and conclusions

(1) Deformation microstructures have been characterized for neutron-irradiated nuclear structural alloys, A533B steel, 316 stainless steel, and Zircaloy-4. Four deformation modes were identified, dislocation cell formation, planar dislocation activity, twinning, and DCD. The results were used to map the extent of strain localization processes in plastic deformation.

(2) In the bcc A533B steel, deformation in the unirradiated and low dose specimens was homogeneous and occurred by interaction and tangling of dislocations. At the middle dose of 0.01 dpa, there was considerable radiation strengthening and the work hardening rate was reduced almost to zero. At the highest dose of 0.89 dpa, black spot radiation damage with a mean defect size of 1.3 nm and concentration of about 6.5×10^{22} m^{-3} was evident. In the two highest dose specimens, prompt plastic instability failures occurred at the yield stress. Channels were observed in the highest dose specimens.

(3) The fluence dependence of the tensile properties of the hcp Zr-4 alloy was found to be similar to that of the A533B steel. For a dose of 0.001 dpa, and in the unirradiated Zr-4, plastic deformation during tension testing occurred by coarsely dispersed planar slip primarily on the slip system

$\{10\bar{1}0\}\langle 11\bar{2}0\rangle$, and to a lesser extent on $\{10\bar{1}1\}\langle 11\bar{2}0\rangle$. At 0.01 dpa, the deformation mode was still planar slip but with stronger participation of $\{10\bar{1}1\}\langle 11\bar{2}0\rangle$. At the two highest doses, where plastic instability failure was initiated at the yield stress, the deformation mode was DCD on the same slip systems. Channel widths were of order 50 nm.

(4) The fcc 316 stainless steel displayed a similar degree of radiation hardening as the A533B steel, yet it retained substantial work hardening and uniform elongation at all doses. In its unirradiated condition, and at the two lowest fluences, where no RDS was visible, it deformed by planar slip on its $\{111\}\langle 110\rangle$ slip systems. As the levels of strain and dose were increased, streaks from fine twins appeared in electron diffraction patterns. For the two highest doses, 0.1 and 0.8 dpa, where black spot-type RDS was observed, dislocation channels were cleared through the RDS. At the highest dose, the dislocation bands and microtwins and channels were superimposed in the deformation bands and were very pronounced. Channel widths were about 20 nm.

(5) Analysis of the fluence (φt) dependence of the increase in tensile yield strength (ΔYS) for all three alloys was made in terms of the relationship $\Delta YS = \alpha(\varphi t)^n$. Values of the radiation hardening exponent, n, were in the range 0.4–0.5 for fluences up to about 3×10^{22} n m^{-2} ($\sim$0.05 dpa), and 0.08–0.15 for higher doses. The reductions in n, which could be read as indications of saturation of radiation damage structure due to cascade overlap, were also found to be concurrent with acceleration of gross strain localization, associated with DCD. This change in deformation mode offers an alternative explanation for the reduced hardening exponent at the higher doses.

Acknowledgments

This research was sponsored by the Nuclear Energy Research Initiative Program, Offices of Nuclear Energy Science and Technology, US Department of Energy, under Contract DE-AC05-00OR22725 with UT-Battelle, LLC. We give special thanks to Drs R.E. Stoller, E.A. Kenik, and S.J. Zinkle for their thorough reviews and comments.

References

[1] F.A. Smidt Jr., NRL Report 7078, Naval Research Laboratory, Washington, DC, 1970.
[2] M.S. Wechsler, The Inhomogeneity of Plastic Deformation, American Society for Metals, 1971.
[3] A. Luft, Prog. Mater. Sci. 35 (1991) 97.
[4] J.V. Sharp, Philos. Mag. 16 (1967) 77.
[5] R.P. Tucker, M.S. Wechsler, S.M. Ohr, J. Appl. Phys. 40 (1969) 400.
[6] T.H. Blewitt, R.R. Coltman, R.E. Jamison, J.K. Redman, J. Nucl. Mater. 2 (1960) 277.
[7] H.J. Frost, M.F. Ashby, Deformation-Mechanism Maps, Pergamon, 1982.
[8] M.F. Ashby, Materials Selection in Mechanical Design, Pergamon, 1992.
[9] S.J. Zinkle, G.E. Lucas, Fusion Mater. Semiannual Progress Report, DOE-ER-0313/34, September 2003, p. 101.
[10] A. Okada, K. Kanao, T. Yoshiie, S. Kojima, Mater. Trans. JIM 30 (1989) 265.
[11] K. Farrell, T.S. Byun, N. Hashimoto, Mapping Flow Localization Processes in Deformation of Irradiated Reactor Structural Alloys, ORNL/TM-2003/63, September 2003.
[12] K. Farrell, T.S. Byun, J.W. Jones. L.T. Gibson, R.G. Sitterson, N. Hashimoto, J.L. Bailey, M.J. Gardner, Small Specimen Procedures for Determination of Deformation Maps, in Small Specimen Test Techniques: Fourth Volume, ASTM STP 1418, American Society for Testing and Materials, 2002, p. 283.
[13] H.R. Higgy, F.H. Hammad, J. Nucl. Mater. 55 (1975) 177.
[14] E.H. Lee, T.S. Byun, J.D. Hunn, K. Farrell, L.K. Mansur, J. Nucl. Mater. 296 (2001) 183.
[15] E.H. Lee, T.S. Byun, J.D. Hunn, M.H. Yoo, K. Farrell, L.K. Mansur, Acta Mater. 49 (2001) 3269.
[16] E.H. Lee, T.S. Byun, J.D. Hunn, M.H. Yoo, K. Farrell, L.K. Mansur, Acta Mater. 49 (2001) 3277.
[17] T.S. Byun, Acta Mater. 51 (2003) 3063.
[18] H. Neuhäuser, R. Rodloff, Acta Met. 22 (1974) 375.
[19] H.L. Heinisch, J. Nucl. Mater. 155–157 (1988) 121.
[20] S.M. Bruemmer, J.I. Cole, J.L. Brimhall, R.D. Carter, G.S. Was, The Sixth International Symposium on Environmental Degradation of Materials in Nuclear Power Systems – Water Reactors – 6th SMIRT, 1993, p. 537.
[21] N. Hashimoto, S.J. Zinkle, A.F. Rowcliffe, J.P. Robertson, S. Jitsukawa, J. Nucl. Mater. 283 (2001) 528.
[22] Ch. Ritschel, A. Luft, D. Schulze, Kristall und Technik 13 (1978) 791.
[23] S. Yoshida, M. Kiritani, Y. Deguchi, N. Kamigaki, Suppl. Trans. JIM 9 (1968) 83.
[24] T. Mori, M. Meshii, Acta Met. 17 (1969) 167.
[25] A. Gysler, G. Lütjering, V. Gerold, Acta Met. 22 (1974) 901.
[26] T.H. Sanders Jr., E.A. Starke Jr., Acta Met. 30 (1982) 927.
[27] I.G. Greenfield, H.G.F. Wilsdorf, J. Appl. Phys. 32 (5) (1961) 827.
[28] U. Essmann, A. Seeger, Phys. Stat. Sol. 4 (1964) 177.
[29] J.L. Brimhall, Trans. Met. Soc. AIME 233 (1965) 1737.
[30] A.H. Cottrell, in: Bristol Conference on Strength of Solids, vol. 30, Phys. Soc., London, 1948.
[31] G.T. Hahn, Acta Met. 10 (1962) 727.
[32] B.N. Singh, A.J.E. Foreman, H. Trinkaus, J. Nucl. Mater. 249 (1997) 103.
[33] R.J. Price, A. Kelly, Acta Met. 12 (1964) 159.

[34] P.J. Jackson, P.D.K. Nathanson, S. African J. Phys. 1 (1978) 7.
[35] M.J. Makin, J.V. Sharp, Phys. Stat. Sol. 9 (1965) 109.
[36] O. Okada, T. Yasujima, T. Yoshiie, I. Ishida, M. Kiritani, J. Nucl. Mater. 179–181 (1991) 1083.
[37] H. Mughrabi, D. Strohle, M. Wilkens, Zeit. fur Metallkunde 72 (5) (1981) 300.
[38] B.A. Cheadle, C.E. Ells, J. vanderKuur, in: Zirconium in Nuclear Applications, ASTM STP 551, Am. Soc. for Testing and Mater., 1974, p. 370.
[39] A.K. Seeger, Proceedings of the Second International Conference on the Peaceful Uses of Atomic Energy, P/989 6 (1958) 250.
[40] S.J. Zinkle, J. Nucl. Mater. 150 (1987) 140.
[41] B.N. Singh, S.J. Zinkle, J. Nucl. Mater. 206 (1993) 212.
[42] M. Eldrup, B.N. Singh, S.J. Zinkle, T.S. Byun, K. Farrell, J. Nucl. Mater. 307–311 (2002) 912.
[43] J.R. Beeler, Flow and Fracture Behavior of Metals and Alloys in Nuclear Environments, ASTM STP 380, Am. Soc. for Testing and Mater., 1964, p. 84.
[44] F. Gao, D.J. Bacon, A.F. Calder, P.E.J. Flewitt, T.A. Lewis, J. Nucl. Mater. 230 (1996) 47.
[45] K. Farrell, T.S. Byun, J. Nucl. Mater. 318 (2003) 274.
[46] S.J. Zinkle, Radiat. Eff. Def. Solids 148 (1999) 447.
[47] T.S. Byun, K. Farrell, Acta Mater. 52 (2004) 1597.
[48] T.S. Byun, K. Farrell, J. Nucl. Mater. 326 (2004) 86.